Understanding Methane Adsorption in Porous Aromatic Frameworks: An FTIR, Raman, and Theoretical Combined Study

ARTICLE *in* THE JOURNAL OF PHYSICAL CHEMISTRY C · APRIL 2014

Impact Factor: 4.77 · DOI: 10.1021/jp412572e

7 AUTHORS, INCLUDING:

Mina Errahali
Amedeo Avogadro University of Eastern Pied…
6 PUBLICATIONS **19** CITATIONS
SEE PROFILE

Giorgio Gatti
Amedeo Avogadro University of Eastern Pied…
54 PUBLICATIONS **556** CITATIONS
SEE PROFILE

Maurizio Cossi
Amedeo Avogadro University of Eastern Pied…
101 PUBLICATIONS **20,098** CITATIONS
SEE PROFILE

THE JOURNAL OF PHYSICAL CHEMISTRY C

Article

pubs.acs.org/JPCC

Understanding Methane Adsorption in Porous Aromatic Frameworks: An FTIR, Raman, and Theoretical Combined Study

M. Errahali, G. Gatti, L. Tei, L. Canti, A. Fraccarollo, M. Cossi, and L. Marchese*

Dipartimento di Scienze e Innovazione Tecnologica and Centro Nano-SiSTeMI, Università del Piemonte Orientale "Amedeo Avogadro", Viale T. Michel 11, 15121 Alessandria, Italy

Supporting Information

ABSTRACT: We present a vibrational study of PAF-302, belonging to the class of porous aromatic frameworks (PAFs), recently synthesized and applied in several applications involving gas adsorption. The precursor, tetrakis(4-bromophenyl) methane (TBPM), and the polymer were studied with FTIR and Raman spectroscopies to investigate the structure of PAF-302, whereas the system after methane adsorption was studied by FTIR, also varying the CH_4 loading, to get some hints on the strength of the interactions with adsorbed methane. Theoretical calculations of the harmonic frequencies of TBPM, methane, and methane/aromatic model systems were performed at high theory level (MP2 with extended basis set) to support the assignment of vibrational bands and to estimate the interactions causing the observed frequency shifts upon methane adsorption. The analysis shows that the polymerization process is essentially complete and that the adsorbed CH_4 molecules interact with two phenyl rings, though stronger interactions can be envisaged. The computed interaction energies are compatible with the isosteric heats of adsorption previously measured for methane in PAF-302. A Grand Canonical Monte Carlo (GCMC) approach was used to simulate CH_4 adsorption isotherms at different temperatures (87−115 K) and in the 0−0.020 bar pressure range, thus allowing us to estimate the loading of methane in the FTIR adsorption study.

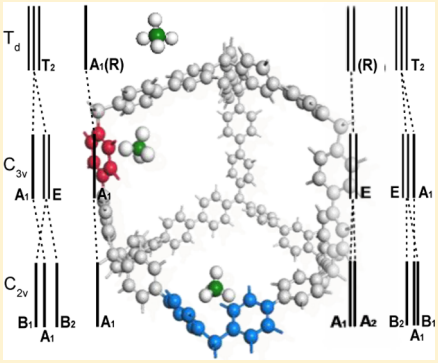

INTRODUCTION

Porous polymers have attracted enormous scientific attention due to their potential applications in several fields, such as separation,[1,2] heterogeneous catalysis,[3,4] and gas storage.[5−9] Such applications are usually based on the presence of a large permanent surface area and narrow pore size distribution, to maximize the gas−solid interactions.[10,11] In 2009, Ben et al.[12] have developed a method to synthesize the first 3D porous aromatic framework (here named PAF-302 but referred to as PAF-1 in the original work), which shows a very high surface area (SBET = 5640 $m^2\ g^{-1}$) and an exceptionally high thermal stability. PAF-30*n* materials consist of a microporous polyphenylene network obtained by the insertion of a variable number (*n*) of phenyl rings between the C−C covalent bonds of diamond-like structure: in the case of PAF-302 biphenyl groups connect two carbon sp^3 atoms.[13] This polymeric system retains the structural features of diamonds and allows sufficient exposure of the faces and edges of phenyl rings, yielding a remarkably high internal surface area. Upon the basis of the same structural motif, in the last 3 years, a series of materials were developed by polymerization of different monomers containing Si, Ge, adamantane, and ethylene in place of the central sp^3 carbon atom.[14−16] Some materials of this class have shown remarkable properties, not only ultrahigh surface area (exceeding 5000 m^2/g) and exceptional physicochemical stability but also high uptake capacities of several gases such as hydrogen, methane, and carbon dioxide.[14] Other studies have treated the functionalization of the PAF-302, to increase the affinity of adsorption of gases. Garibay et al.,[17] for example, described the synthesis of methyl-, hydroxymethyl-, and phthalimidomethyl-functionalized analogues of PAF-302, whereas Zhou and co-workers[18] reported the postsynthesis modification (PSM) of PAF-302 to yield sulfonated and chloromethyl derivatives. In connection with its impressive surface area, PAF-302 exhibits high uptakes of CH_4 (18 $cm^3\ g^{-1}$ at 1 bar and 273 K), H_2 (7.0 wt % at 48 bar and 77 K), and CO_2 (1.3 g g^{-1} at 40 bar and 298 K).[8]

Computational results, obtained by our group using grand canonical Monte Carlo simulations, established the potential use of these materials in the automotive field. The methane storage in PAF-302 is 5 times larger than in the compressed gas at about 60 bar and 298 K, and even at 280 bar, the adsorbed gas is 43% more dense,[19] making the proposed applications of PAF-302 for methane storage very promising.

In this contribution, FTIR and Raman spectroscopies, along with ab initio calculations, are employed to describe the PAF-302 vibrational features and investigate the interactions of methane with the surface of the porous framework. Upon adsorption, methane vibrational modes are shifted due to the host−guest interactions with the surface: several studies have

Received: December 23, 2013
Revised: April 17, 2014
Published: April 22, 2014

   dx.doi.org/10.1021/jp412572e | J. Phys. Chem. C 2014, 118, 10053−10060

been performed on zeolites,[20] silica,[21,22] and oxides,[23] but only few works have been done on carbon-based adsorbents such as activated carbon and C_{60} fullerenes.[24,25]

The vibrational spectra of the polymer have been interpreted by comparison with the spectra of tetrakis(4-bromophenyl) methane (TBPM), the precursor used in the PAF-302 synthesis, whose vibrational frequencies have been assigned with the help of theoretical calculations. The shift of the methane vibrational frequencies upon adsorption can be related to the strength of molecule/surface interactions as well as to the decrease of the molecular symmetry (T_d in the the gas phase). Also in this case, the use of simplified models studied at the ab initio level has greatly supported the experimental analysis.

EXPERIMENTAL

Materials and Methods. All chemicals were purchased from either Sigma Aldrich Co. or Alfa Aesar Co. and were used without purification for the PAF-302 synthesis. Tetrakis(4-bromophenyl) methane (TBPM) was synthesized according to literature procedure.[26] Gas CH_4 (Rivoira S.p.A., 99.995%) and CD_4 (Cambridge Isotope Laboratories, Inc. C.N. CDLM-1616-0 with deuterium pure grade 99.7%) were employed for the infrared adsorption measurements. PAF-302 was synthesized following the procedure reported by Ben and co-workers:[12] in particular, 1,5-cyclooctadiene (COD, 1.05 mL, 8.32 mmol) was added to a solution of bis(1,5-cyclooctadiene)nickel(0) ([Ni-(cod)$_2$, 2.25 g, 8.18 mmol) and 2,2′-bipyridyl (1.28 g, 8.18 mmol) in anhydrous DMF (120 mL), and the mixture was heated under Ar at 353 K for 1 h. Tetrakis(4-bromophenyl)-methane (1g, 1.57 mmol) was added to the resulting purple solution, and the mixture was stirred at 353 K overnight to obtain a deep purple suspension. After cooling to room temperature, concentrated HCl was added to the mixture. After filtration, the residue was washed with H_2O (5 × 30 mL), THF (5 × 30 mL), and $CHCl_3$ (5 × 30 mL), respectively, and dried in a vacuum to give PAF-302 (482 mg, 96% yield).

Solid State Nuclear Magnetic Resonance Spectroscopy. The solid state NMR (SS-NMR) spectrum of PAF-302 was acquired on a Bruker Avance III 500 spectrometer and a wide bore 11.7 T magnet with operational frequencies for ^{13}C of 125.77 MHz. A 7 mm double resonance probe with magic-angle spinning (MAS) was employed in the experiment. The sample was packed on a Zirconia rotor and spun at a MAS rate of 5 kHz. For the $^{13}C\{^1H\}$ CPMAS experiment, the magnetic fields υ_{rf}^{H} of 42 and 23 kHz were used for initial excitation and decoupling, respectively. During the cross-polarization (CP) period the ^1H radio frequency (RF) field υ_{rf}^{H} was ramped using 100 increments, whereas the ^{13}C RF field υ_{rf}^{C} was maintained at a constant level. During the acquisition, the protons were decoupled from the carbons by using a TBPM decoupling scheme, and the CP contact time of 5 ms was used. The relaxation delay between accumulations was 2 s, and all chemical shifts are reported using δ scale and are externally referenced to TMS at 0 ppm.

X-ray Diffractogram (XRD). The XRD of PAF-302 was recorded on an unoriented ground powder with a Thermo ARL "XTRA-048 diffractometer" with Cu Kα (k = 1.54 Å) radiation.

Thermogravimetric Analysis. Analysis was performed on a Setaram SETSYS Evolution instrument under argon (gas flow 20 mL/min), heating the PAF-302 sample to 1173 K with a rate of 5 K/min.

Scanning Electron Microscopy (SEM). SEM images were recorded on a Quanta 200 FEI scanning electron microscope equipped with EDAX EDS attachment, using a tungsten filament as the electron source at 20 keV.

Infrared Spectra. IR spectra of materials in the form of self-supporting pellets were collected under vacuum conditions (residual pressure <10^{-5} Torr; 1 Torr = 133.33 Pa) using a Bruker Equinox 55 spectrometer equipped with a pyroelectric detector (DTGS type) with a resolution of 2 cm^{-1}. Before gas adsorption experiments, samples were outgassed at 473 K at a heating rate of 5 K/min, for 12 h in the IR cell directly connected to the vacuum line. After the thermal treatment, the samples were then cooled to 110 K for the collection of IR spectra at 20 mbar of CH_4 and progressively decreased gas pressures. The same experiment was performed using CD_4 gas. Curve fitting of the stretching band in the 2350−2150 cm^{-1} range for adsorbed CD_4 was performed with the local least squares using OPUS software (Bruker Optics). Gaussian functions were used at fixed positions for each component of the spectra obtained at different CD_4 dosages.

Raman Spectra. Raman spectra were recorded on as-prepared powders using a Bruker RFS 100 FT spectrophotometer with a Nd_3+YAG laser source (k = 1064 nm) and a laser power of 50 mW: 2000 scans were collected for each spectrum.

N_2 Physisorption. N_2 physisorption measurement was carried out at 77 K in the relative pressure range from 1×10^{-6} to $1P/P_0$ by using a Quantachrome Autosorb1MP/TCD instrument. Prior to the analysis, the sample was outgassed at 473 K for 16 h (residual pressure lower than 10^{-6} Torr). The PAF-302 sample showed a specific surface area (SSA) of 4200 m^2/g as found by using the Brunauer−Emmett−Teller equation, in the relative pressure range from 0.05 to $0.15P/P_0$.

Theoretical Calculations. The calculations were performed both at the DFT (density functional theory) level and with the correlated MP2 (second-order Moller−Plesset perturbation) method. DFT was used with the B3LYP functional and 6-311G(2d,2p) basis set for the geometry optimization and harmonic frequencies calculation on TBPM, while the more accurate and expensive MP2 method was used with the 6-311+G(d,p) basis set on CH_4/aromatic system models. The methane adsorption isotherms at different temperatures between 87 and 115 K and pressures up to 0.020 bar were simulated using the sorption module included in the Materials Studio package, in a series of grand canonical Monte Carlo (GCMC) simulations. The isotherms were computed with a modified version of the Dreiding force field: the Lennard-Jones parameters for nonbonded interactions of H and sp^3 and sp^2 C atoms were adjusted to fit experimental and high-level ab initio data according to the procedure described in refs 19 and 27.

RESULTS AND DISCUSSION

FTIR and Raman Spectroscopy of PAF-302. PAF-302 appears as an off-white powder insoluble in common organic solvents. Its solid-state ^{13}C CP-MAS NMR spectrum (Figure S1 in Supporting Information) is consistent with that previously[12] reported for PAF-302 and suggests a regular short-range organization of biphenyl groups around tetrahedral carbon atoms. The powder X-ray diffraction (PXRD) profile (Figure S2 in Supporting Information), however, indicates that the polymer lacks long-range periodicity probably because the phenyl rings are not perfectly aligned with each other in the

dx.doi.org/10.1021/jp412572e | J. Phys. Chem. C 2014, 118, 10053−10060

particle. Thermogravimetric analysis (TGA) confirmed the good thermal stability of the polymer and its high temperature of decomposition above 450 °C in argon atmosphere (Figure S3 in Supporting Information). Scanning electron microscopy (SEM) images of PAF-302 (Figure S4 in Supporting Information) indicate that aggregated particles of 100−300 nm and a platelike morphology are essentially present.

3D molecular models of TBPM (a) and the PAF-302 unit cell (b) are shown in Figure 1.

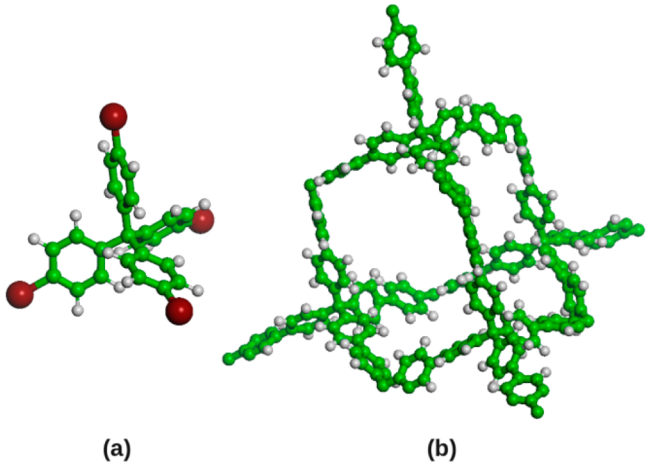

Figure 1. Molecular model of (a) TBPM and (b) the PAF-302 unit cell.

In Figure 2 we report the FTIR vibrational spectrum of the PAF-302 polymer in the region 3300−450 cm^{-1} along with the spectrum of the precursor, TBPM.

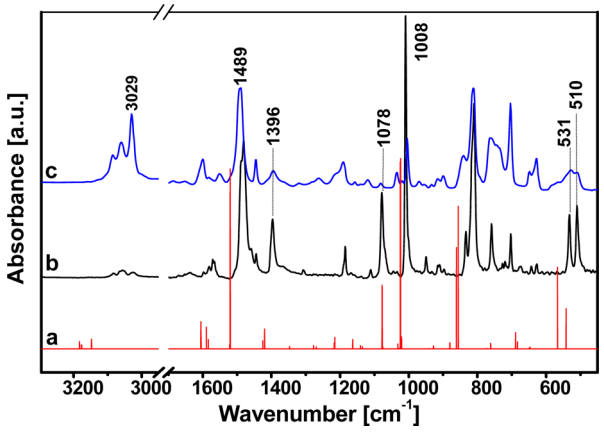

Figure 2. FTIR spectra in the region 3300−450 cm^{-1} of: (a) DFT spectrum of TBPM calculated in harmonic approximation at the B3LYP/6−311G(2d,2p) level; (b) and (c) experimental spectra of TBPM and PAF-302 in the KBr pellet, respectively.

TBPM vibrational bands were assigned by comparison with a theoretical spectrum calculated at the B3LYP/6-311G(2d,2p) level at the molecular geometry previously optimized: the main components are listed in Table 1. From the data in Table 1 and Figure 2, one can see that the theoretical (a) and experimental (b) TBPM spectra are in good agreement, presenting only a small shift due to the harmonic approximation in the calculated results.

The FTIR spectrum of TBPM generally shows sharp bands because of the crystalline nature of the compound. Three very weak bands are found in the high-frequency region at 3085, 3059, and 3029 cm^{-1}, which are assigned to the CH stretching vibrations of the aromatic rings on the basis of the calculated spectrum and in agreement with the literature.[28,29] Likewise, based on the computed spectrum, in the low-frequency region the bands falling at 1481 and 1396 cm^{-1} involve "semicircle stretching pair" modes of the aromatic rings. The band at 1078 cm^{-1} is an almost pure C−Br stretching mode, whereas the intense and sharp band at 1008 cm^{-1} is assigned to the C−C bending of the aromatic rings coupled with C−H bending and C−Br stretching vibrations. At lower frequencies the bands with medium intensity at 531 and 510 cm^{-1} are assignable to the out-of-plane quadrant ring bending deformations somehow coupled with the C−Br deformation.

These results have allowed us to assign with more precision the IR bands of the PAF-302 polymer (Figure 2c). The comparison between PAF-302 and TBPM spectra shows that in general the bands of the polymer become broader, change in intensity, and slightly shift in the position. Indeed, after the polymerization reaction the high-frequency band intensity largely increases due to the change of the local dipole moment related to the aromatic ring asymmetric CH stretching. Furthermore, the bands at 1396, 1008, 531, and 510 cm^{-1} assigned to the aromatic ring stretching and bending (the last three being coupled to C−Br vibrations) undergo a drastic reduction in their intensities in the PAF-302 polymer: it can be thus inferred that the dipole moment of these modes is strongly influenced by the presence of bromine atoms in the TBPM precursor. The main fingerprint of the polymerization is, however, related to the band at 1078 cm^{-1} due to the C−Br vibration, which diminished to an undetected level in the PAF-302 spectrum, suggesting essentially complete reaction of the starting TBPM.

The PAF-302 Raman spectrum (Figure 3) was also interpreted with the help of both the computed and the experimental TBPM spectra: Table 2 summarizes the assignments of the main vibrational modes. In the high wavenumber region the TBPM spectrum (Figure 3, curve b) is characterized by an intense broad absorption at 3058 cm^{-1} with an evident weaker band at 3076 cm^{-1} and a shoulder at lower wavenumber. The bands in this region can be easily assigned to the C−H stretching vibrations of the aromatic rings on the basis of the calculated spectrum (Figure 3, curve a). At low frequency, the TBPM spectrum shows a band at 1580 cm^{-1} due to the ring quadrant stretching, whereas the peaks at 1187 and 1137 cm^{-1} are due to the asymmetric and symmetric stretching of the quaternary carbon, respectively. As in the infrared spectrum, the strong band at 1078 cm^{-1} is assigned to the C−Br stretching, whereas at lower frequencies the band at 724 cm^{-1} is due to the in-plane quadrant bending of the aromatic ring coupled to C−Br stretching.

The comparison between PAF-302 and TBPM spectra (Figure 3, curves c and b, respectively) at high frequency shows a significant decrease in the intensity of the bands referred to C−H stretching vibrations in agreement with the fact that upon polimerization the symmetry of the TBPM is removed and the CH stretching vibrations become asymmetric (strong IR activity, as clearly seen in Figure 2). Remarkably, in the low-frequency region, the bands at 1078 and 724 cm^{-1} of the precursor, assigned to vibrations involving the bromine atoms, are absent in the spectrum of the polymer PAF-302, indicating

dx.doi.org/10.1021/jp412572e | J. Phys. Chem. C 2014, 118, 10053−10060

Table 1. IR Vibrational Modes of the TBPM Calculated Spectrum Compared to Those of the TBPM and PAF-302 Experimental Spectra[a]

vibrational mode	TBPM calcd freq. [cm^{-1}]	TBPM exptl freq. [cm^{-1}]	PAF-302 exptl freq. [cm^{-1}]
stretch aromatic C−H	3183, 3176, 3147	3083(vw), 3057(vw), 3026(vw)	3085(w), 3059(m), 3029(s)
ring quadrant stretch	1605−1583	1603−1555	1621−1531
semicircle stretch pair	1520, 1420	1481(s), 1396(m)	1489(s), 1394(w)
in-plane C−H bend	1215	1185	1190
C−Br stretch	1077	1078(m)	1081(vw)
ring C−C bend + C−H bend + C−Br stretch	1024	1008(vs)	1005(m)
ring and C−H out-of-plane bend	861, 761	810(s), 759	812(m), 761
in-plane ring bend	689	702	703
out-of-plane quadrant ring bend + C−Br bend	566, 541	531(m), 510(m)	557−497(w)

[a]vs = very strong, s = strong, m = medium, w = weak, and vw = very weak.

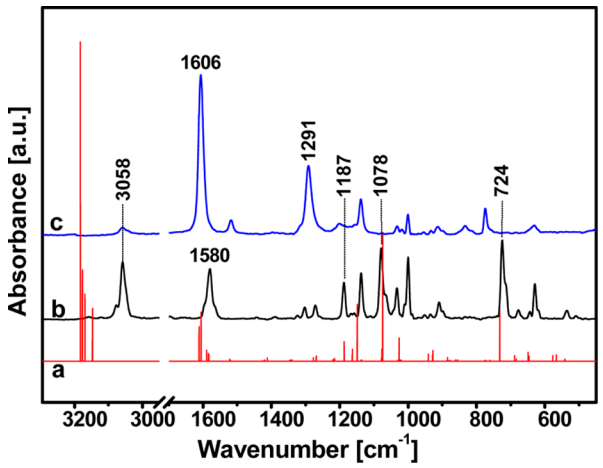

Figure 3. Raman spectra in the 3300−450 cm^{-1} region: (a) TBPM theoretical spectrum calculated in harmonic approximation at the B3LYP/6-311G(2d,2p) level; (b) and (c) experimental spectra of TBPM and PAF-302, respectively.

a complete polymerization in full agreement with the IR results. Another mark of the polymerization, only present in the Raman spectrum, is given by the intense band at 1291 cm^{-1}, which is absent in the precursor: it has been assigned to the stretching of the C−C bond which is formed after the coupling between the aromatic rings.

CH_4 Adsorption on PAF-302. This section deals with the analysis of the interaction between methane and the PAF-302 polymer. IR modes of adsorbed methane depend on host−guest interactions, which are strictly related to the chemical nature of the surface: on zeolite[20] and oxide[23] materials methane molecules are primarily polarized by the strong electric fields generated by ionic sites, whereas on silica and alumina methane molecules interact with surface hydroxyl groups.[21,22] However, for carbon-based adsorbents[24,25] like PAF-302, only van der Waals interactions are envisaged, and we use a combined experimental and computational approach to evaluate this type of interaction. The calculations were performed on model systems constituted by complexes of methane with both *p*-xylene and ditolylmethane (vide infra) to describe the local interactions of methane with one or two aromatic rings; both interaction energies and vibrational frequencies were computed for the complexes.

Methane was adsorbed at 110 K on PAF-302 pretreated in a vacuum at 473 K (Figure 4, curve a), and the infrared spectra were recorded at variable pressure: the maximum CH_4 pressure was 7 mbar (curve b). The amount of adsorbed methane was varied by progressively decreasing the gas pressure after reaching the equilibrium for each step (spectra c−n). The three characteristic C−H stretching bands of the aromatic rings of PAF-302 described in the previous section at 3085, 3059, and 3029 cm^{-1} are slightly shifted to lower frequency upon exposure to CH_4 at 110 K. At the same time two new bands appear at 3002 and 2900 cm^{-1} with strong and very weak intensity, respectively. At low frequency a new strong band also appears at 1300 cm^{-1}. The progressive reduction of pressure (curves c−n) causes the decrease in the intensity of the three bands until complete disappearance, and simultaneously the C−H stretching bands shift back to higher frequency. To detect if other bands of adsorbed methane are masked by the structural bands of the material, a difference spectrum at an

Table 2. Raman Vibrational Modes of the TBPM Calculated Spectrum Compared to Those of the TBPM and PAF-302 Experimental Spectra[a]

vibrational mode	TBPM calcd freq. [cm^{-1}]	TBPM exptl freq. [cm^{-1}]	PAF-302 exptl freq. [cm^{-1}]
stretch aromatic C−H	3183−3147	3088−3031	3074−3039
ring quadrant stretch	1612−1580	1580(s)	1606(vs), 1517(w)
ring sextant stretch	1269	1271	–
C−C biphenyl bond stretch	–	–	1291
asym. C−C quaternary carbon stretch	1187	1187(m)	1201(vw)
sym. C−C quaternary carbon stretch	1150	1137	1138
C−Br stretch	1076	1078(s)	–
ring C−C bend + out-of-plane CH bend	1027	1000(m)	1000(w)
in-plane quadrant bend + C−Br stretch	732	724(s)	–
in-plane quadrant bend	646	630(m)	630(w)

[a]vs = very strong, s = strong, m = medium, w = weak, and vw = very weak.

dx.doi.org/10.1021/jp412572e | J. Phys. Chem. C 2014, 118, 10053−10060

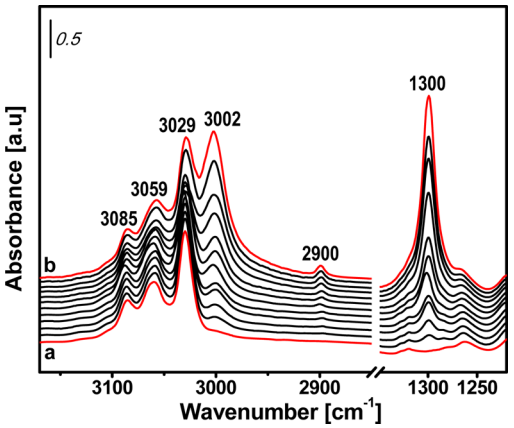

Figure 4. IR spectra of methane adsorbed at 110 K on PAF-302: (a) bare PAF-302 sample outgassed at 473 K, (b) PAF-302 in contact with 7 mbar of CH_4, and (c–n) spectra recorded by decreasing progressively the methane pressure (5.7, 4.9, 4.3, 3.4, 2.3, 1.4, 0.7, 0.4, 0.2, and 0.07 mbar).

equilibrium pressure of 7 mbar is reported in Figure 5 (spectrum obtained by subtracting curve a from b of Figure 4).

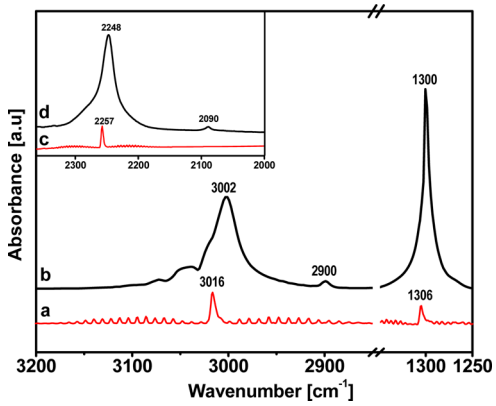

Figure 5. IR spectra of (a) CH_4 gas and (b) difference spectrum (b–a of Figure 4). In the inset are reported (c) CD_4 gas and (d) difference spectrum at equilibrium pressure of 7 mbar CD_4.

Besides the band at 3002 cm^{-1}, the spectrum of adsorbed CH_4 clearly shows other components at higher wavenumber; however, the shape and position of the bands in this region cannot be detected with precision because of the shift of the IR peaks of the PAF-302 structure upon methane adsorption (vide supra): for this reason the difference spectrum presents false minima/maxima. This was confirmed by adsorbing deuterated methane (CD_4), whose absorptions fall in the region 2350–2000 cm^{-1} free from the bands of the PAF structure (inset of Figure 5). The most intense band in this region is found at 2248 cm^{-1}: the ratio between the wavenumber of the bands at 3002 and 2248 cm^{-1} is 1.34, in agreement with the hydrogen/deuterium substitution, thus suggesting that the two absorptions are related to the same vibrational mode. It is clear that the band at 2248 cm^{-1} has a broad shoulder at higher wavenumber, and this shape should be similar to that of the adsorbed CH_4. In other words, several heavily overlapped components are found in the region of CH stretching vibrations when methane is adsorbed on PAF-302: for the assignment of these bands on the basis of the group theory (i.e., the classification of normal modes) the possible local symmetry of the adsorbed molecules has to be considered.

Methane is a tetrahedral molecule (symmetry point group T_d) which exhibits four normal modes of vibration according to the symmetry of the associated normal coordinates, as reported in the scheme of Figure 6. The PAF-302 polymer is characterized by a 3D structure where methane can interact simultaneously with faces and edges of phenyl rings, and monodentate (local C_{3v} symmetry) and bidentate (local C_{2v} symmetry) configurations of methane molecules are possible (see schemes in Figure 6).

Upon methane adsorption the forbidden modes (that would be normally detected by Raman spectroscopy only) may become observable in the infrared spectra because of surface interactions. When the symmetry is decreased to C_{3v} the A_1 Raman mode of the free methane becomes IR active and the triply degenerate T_2 vibrations split into two IR active modes (A_1 and E). When a bidentate structure is considered, the symmetry is lowered to C_{2v}, and all the vibrational modes become IR active and nondegenerate. This scheme based on simple symmetry considerations can be enhanced by using molecular models for the methane/PAF interactions, possibly providing some quantitative predictions: in Figure 7 we show two complexes of CH_4 with *p*-xylene and ditolylmethane, representative of the local C_{3v} and C_{2v} symmetries, respectively. Both geometry optimization and harmonic frequency calculation were performed at the MP2 level with the 6-311+G(d,p) basis set: for similar methane/aromatic complexes, it has been shown that the MP2 method with extended basis is necessary for an accurate calculation of the vibrational pattern.[30]

The calculated interaction energies and frequency shifts for the CH_4/*p*-xylene and CH_4/ditolylmethane clusters are reported in Table 3. Note that the cluster geometries do not match exactly the symmetry group of the ideal model since a small energy decrease is usually associated to a relaxation of the symmetry constraints: in particular, in the cluster with *p*-xylene the methane C–H points to one of the aromatic carbon atoms instead of the ring center. This is a well-known feature of the methane/benzene complexes, where the symmetry of the optimized structure strongly depends on the calculation level: with MP2, when the basis set is sufficiently enlarged, the structure passes from C_{3v} (C–H pointing to the center of the ring) to the "pseudo-C_{3v}" that we have obtained. In any case the potential energy surface is very flat with respect to the orientation of the C–H bond, which is likely to switch from one aromatic carbon to another quickly.

With these limitations, the data in Table 3 can be compared to the symmetry model. The triply degenerated asymmetric stretching mode of free methane (computed at 3212 cm^{-1}) is split into two components in the methane/*p*-xylene complex (a single band almost unshifted, at 3213 cm^{-1}, and a doubly degenerate band downshifted by 12 cm^{-1}) and further split into three single absorptions in the cluster with ditolylmethane, the lower component (B_2 symmetry) being shifted −22 cm^{-1}. The symmetric C–H stretching mode, IR forbidden in free methane, appears in the clusters as a consequence of the decrease of the symmetry from T_d to C_{3v} and C_{2v}, where the A_1 symmetry vibration is IR active: the calculated frequency of this mode is downshifted by 8 and 11 cm^{-1} in the clusters with *p*-xylene and ditolylmethane, respectively. It is also noteworthy that the interaction energies estimated at the MP2 level agree quite well with the experimental isosteric heat of adsorption of

dx.doi.org/10.1021/jp412572e | J. Phys. Chem. C 2014, 118, 10053–10060

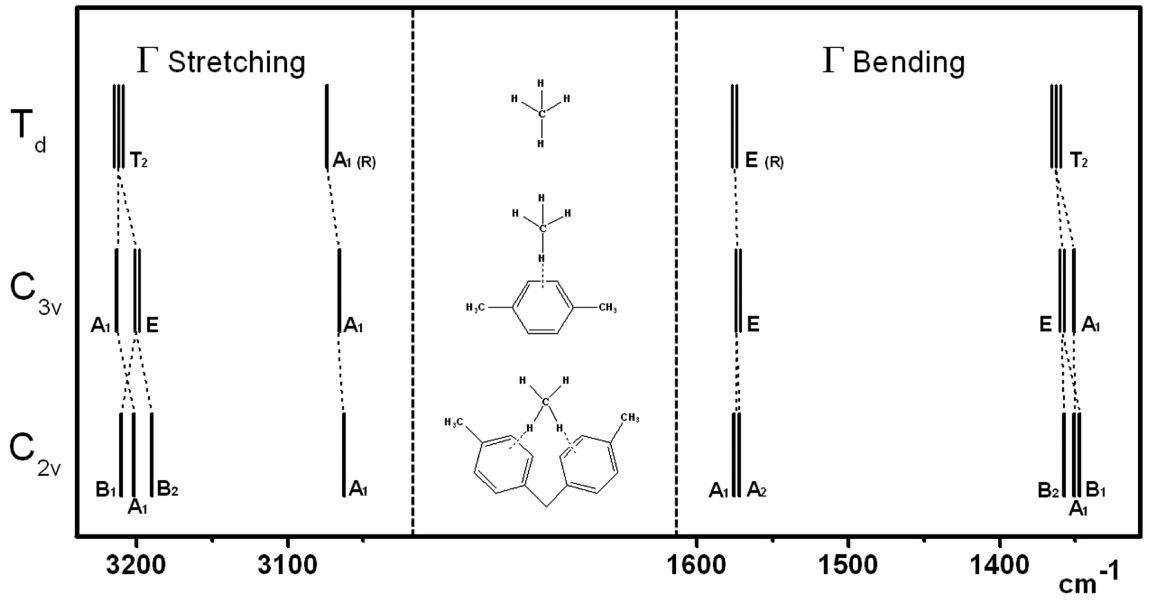

Figure 6. Representation of the theoretical stretching and bending harmonic frequencies of free CH_4 (T_d symmetry), *p*-xylene−methane (C_{3v} symmetry), and ditolylmethane−methane (C_{2v} symmetry) structures. The normal modes of vibration are classified on the basis of the point group to which the adsorbed methane belong.

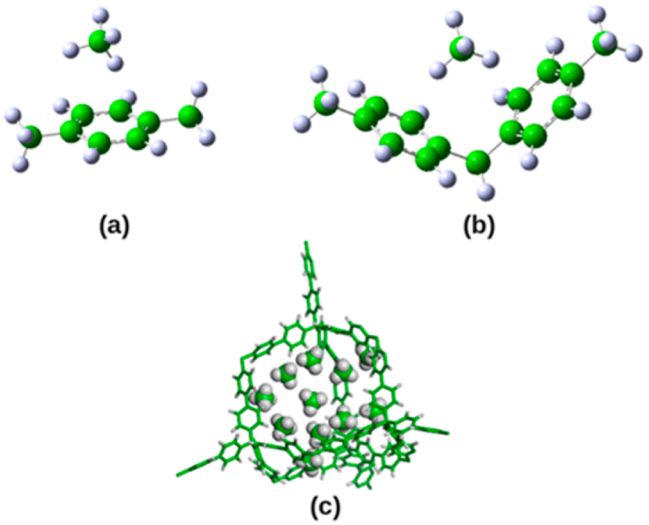

Figure 7. Model systems used for the calculation of harmonic frequencies: (a) methane/*p*-xylene cluster and (b) methane/ditolylmethane cluster. A model of PAF-302 crystalline structure with a number of adsorbed CH_4 molecules, to illustrate the variety of possible positions inside the porous material, is also shown in (c).

methane in PAF-302, measured by Ben and co-workers who obtained around 3.35 kcal/mol.[8]

The experimental vibrational frequencies of free methane and methane adsorbed on PAF-302 are reported in Table 4, where the case of deuterated methane is also considered.

The very intense band at 3002 cm^{-1} with a shoulder at higher wavenumber is assigned to the stretch ν_3 of adsorbed CH_4 shifted by 14 cm^{-1} with respect to the vibration at 3016 cm^{-1} in the methane gas (Figure 5, curve b). As described above, this vibrational mode is triply degenerated in gaseous methane, while the degeneration is removed when the interactions with the surface lower the symmetry, in agreement with the broad asymmetric band observed in the spectrum of adsorbed methane. It is of note that the calculated shifts are

Table 3. Interaction Energies and Harmonic Frequencies Computed at the MP2/6-311+G(d,p) Level[a]

	interaction energy (kcal/mol)		harmonic frequency (cm^{-1})		
			this work		ref 30
	this work[b]	ref 30	ν_3	ν_1	ν_1
methane	--	--	3212	3074	3058
methane/*p*-xylene	−2.37	−2.25	3213, 3200	3066 (−8)	3050 (−8)
methane/ditolylmethane	−3.91	--	3210, 3202, 3190	3063 (−11)	--

[a]In parentheses the frequency shifts with respect to free methane. Some results from ref 30, obtained at the MP2 level with a larger basis set, are reported for comparison. [b]Counterpoise correction to BSSE included.

−12 and −22 cm^{-1} for "pseudo C_{3v}" and C_{2v} complexes (Table 3), respectively. This accounts for the very broad band found in the experimental spectrum, which is thus formed of several unresolved components whose nature cannot be identified with precision. However, it is likely that either monodentated or bidentate adducts can be formed upon adsorption of methane on PAF-302, notwithstanding that other host−guest interactions are also possible as described in Figure 7c.

The symmetric stretching (ν_1) mode, which becomes IR active after the interaction with the PAF-302 framework, is characterized by a weak band at 2900 cm^{-1}: the corresponding frequency in the free molecule, visible in the Raman spectrum of gaseous methane, falls at 2917 cm^{-1}.[31] Upon adsorption then the ν_1 mode is shifted by −17 cm^{-1}, to be compared to the theoretical shifts of −8 and −11 cm^{-1} for interactions with one or two aromatic rings, respectively. Also considering the errors due to the harmonic approximation in the theoretical results (strongly reduced when frequency *shifts* are computed, anyway), the measured ν_1 shift indicates a strong interaction

dx.doi.org/10.1021/jp412572e | J. Phys. Chem. C 2014, 118, 10053−10060

Table 4. IR Frequencies and Shifts upon CH_4 and CD_4 Adsorption on PAF-302[a]

mode	CH_4 (gas) [cm^{-1}]	CH_4 (ads.) [cm^{-1}]	shift, $\Delta\nu/cm^{-1}$	CD_4 (gas) [cm^{-1}]	CD_4 (ads.) [cm^{-1}]	shift, $\Delta\nu/cm^{-1}$
ν_1 (A_1)	2917[a] (R)	2900	−17	2101[a] (R)	2090	−11
ν_2 (E)	1533[a] (R)	[b]	-	1090[a] (R)	[b]	-
ν_3 (T_2)	3016 (IR)	3002	−14	2257 (IR)	2248	−9
ν_4 (T_2)	1306 (IR)	1300	−6	995 (IR)	990	−5

[a]Ref 31. [b]Not detected because masked by PAF-302 structural vibrations.

of methane with PAF-302 aromatic moieties, with more than two phenyl rings affecting this vibration mode apparently.

Finally, in the low-frequency region the ν_4 bending mode at 1306 cm^{-1} is shifted by −6 cm^{-1} with respect to free CH_4 gas. Because the deformation modes are less perturbed when the molecule is adsorbed, this result is consistent with the PAF/CH_4 interactions previously described.

Monte Carlo Adsorption Isotherms. To correlate the information from FTIR spectra with the interactions experienced by the single methane molecules, it is of great interest to evaluate the actual number of gas molecules adsorbed in PAF-302 pores at the various pressures. The adsorption isotherms at different temperatures in the range 87−115 K were simulated with the grand canonical Monte Carlo (GCMC) method, using a force field specifically designed to study methane adsorption in PAF materials, as detailed in ref 19; the isotherms, for pressures up to 0.020 bar, are reported in the Supporting Information (Figure S5).

At 110 K, i.e., the temperature at which the FTIR spectra discussed above were recorded, the unit cell of model PAF-302 contains about 10 molecules at 0.001 bar and 140 molecules at saturation, above 0.010 bar. These quantities have to be reduced by around 20% in the actual sample, whose specific area is ca. 4200 m^2/g, compared to ca. 5500 m^2/g of the ideal material used in GCMC simulations.[19] Considering that the PAF-302 unit cell contains 4 sp^3 carbon atoms, or equivalently 8 biphenyl moieties, we estimate that the methane molecules/biphenyl ratio is approximately 1 at 0.001 bar and 14 at saturation.

Then at low pressure the guest molecules can be considered isolated and interacting solely with the aromatic moieties (host−guest interactions), while at saturation marked guest−guest interactions arise: this agrees with the behavior of the CD_4 spectra discussed above (see Figure 5), where the band centered at 2248 cm^{-1} can be decomposed into Gaussian-type contributions. As shown in the Supporting Information (Figure S6), a good fit is obtained using four components: the broader component, centered at the lowest wavenumber, can be associated to guest−guest, liquid-like interactions, and the weight of this band increases markedly at high pressure, as expected.

CONCLUSIONS

The vibrational spectra of PAF-302 and its adduct with methane have been recorded and resolved, to investigate the structure of the porous framework and the interactions with the adsorbed gas. FTIR and Raman techniques were employed, along with theoretical calculations at the MP2 level with an extended basis set. The PAF-302 spectrum was compared with that of the precursor TBPM, whose vibrational pattern was resolved with the aid of the computed harmonic frequencies, showing that the polymerization reaction can be considered complete.

FTIR spectra were recorded after adsorption of CH_4, with different gas loadings: they were resolved by comparison with the spectra of adsorbed CD_4 and with the help of theoretical calculations on model systems, that is, methane interacting with *p*-xylene and with ditolylmethane in "pseudo C_{3v}" and C_{2v} local symmetry, respectively. A simple model based on the symmetry reduction passing from gaseous to adsorbed methane allowed us to predict the structure of the vibrational bands upon adsorption: the calculations on the molecular models provided an estimate of the expected frequency shifts. On the basis of these results, the spectra recorded after adsorption indicate multiple interactions between methane and the PAF surface, where one or two phenyl rings (i.e., monodentate or bidentate adducts, respectively) are involved. The computed interaction energies for the methane/ditolylmethane cluster are in good agreement with the experimental isosteric heat of adsorption of CH_4 in PAF-302. Finally, a GCMC approach was used to simulate the methane adsorption isotherm in the conditions adopted for FTIR experiments (i.e., 110 K and 0−0.020 bar), and the simulated isotherms allowed the determination of the methane loading for each FTIR spectrum, thus corroborating the definition of the host−guest and guest−guest interactions in the methane/PAF-302 system.

ASSOCIATED CONTENT

Supporting Information

Characterization of the PAF-302 material (1. Solid-state ^{13}C MAS NMR; 2. Powder XRD; 3. TGA curve; 4. SEM micrographs; 5. GCMC adsorption isotherms of CH_4 on PAF-302; 6. IR difference spectra of CD_4 adsorbed on PAF-302). This material is available free of charge via the Internet at http://pubs.acs.org.

AUTHOR INFORMATION

Corresponding Author

*E-mail: leonardo.marchese@mfn.unipmn.it.

Notes

The authors declare no competing financial interest.

ACKNOWLEDGMENTS

This work was greatly improved by many helpful discussions with Geo Paul and Gabriele Alessandro Rolla (Università del Piemonte Orientale, Dipartimento di Scienze e Innovazione Tecnologica). The financial support by OMB-Saleri and SOL-Group is gratefully acknowledged.

REFERENCES

(1) McKeown, N. B.; Budd, P. M. Polymers of intrinsic microporosity (PIMs): organic materials for membrane separations, heterogeneous catalysis and hydrogen storage. *Chem. Soc. Rev.* **2006**, *35*, 675−683.

(2) Li, B.; Su, F.; Luo, H.-K.; Liang, L.; Tan, B. Hypercrosslinked microporous polymer networks for effective removal of toxic metal ions from water. *Microporous Mesoporous Mater.* **2011**, *138*, 207−214.

(3) Du, X.; Sun, Y.; Tan, B.; Teng, Q.; Yao, X.; Su, C.; Wang, W. Tröger's base-functionalised organic nanoporous polymer for heterogeneous catalysis. *Chem. Commun.* **2010**, *46*, 970−972.
(4) Dang, D.; Wu, P.; He, C.; Xie, Z.; Duan, C. Homochiral metal-organic frameworks for heterogeneous asymmetric catalysis. *J. Am. Chem. Soc.* **2010**, *132*, 14321−14323.
(5) Furukawa, H.; Yaghi, O. M. Storage of Hydrogen, Methane, and Carbon Dioxide in Highly Porous Covalent Organic Frameworks for Clean Energy Applications. *J. Am. Chem. Soc.* **2009**, *131*, 8875−8883.
(6) McKeown, N. B.; Gahnem, B.; Msayib, K. J.; Budd, P. M.; Tattershall, C. E.; Mahmood, K.; Tan, S.; Book, D.; Langmi, H. W.; Walton, A. Towards Polymer-Based Hydrogen Storage Materials: Engineering Ultramicroporous Cavities within Polymers of Intrinsic Microporosity. *Angew. Chem.* **2006**, *118*, 1836−1839.
(7) Wood, C. D.; Tan, B.; Trewin, A.; Su, F.; Rosseinsky, M. J.; Bradshaw, D.; Sun, Y.; Zhou, L.; Cooper, A. I. Microporous Organic Polymers for Methane Storage. *Adv. Mater.* **2008**, *20*, 1916−1921.
(8) Ben, T.; Pei, C.; Zhang, D.; Xu, J.; Deng, F.; Jing, X.; S. Qiu, S. Gas Storage in Porous Aromatic Frameworks (PAFs). *Energy Environ. Sci.* **2011**, *4*, 3991−3999.
(9) Morris, R. E.; Wheatley, P. S. Gas Storage in Nanoporous Materials. *Angew. Chem., Int. Ed.* **2008**, *47*, 4966−4981.
(10) Yushin, G.; Dash, R.; Jagiello, J.; Fischer, J. E.; Gogotsi, Y. Carbide-Derived Carbons: Effect of Pore Size on Hydrogen Uptake and Heat of Adsorption. *Adv. Funct. Mater.* **2006**, *16*, 2288−2293.
(11) Rodríguez-Reinoso, F.; Nakagawa, Y.; Silvestre-Albero, J.; Juárez-Galán, J. M.; Molina-Sabio, M. Correlation of methane uptake with microporosity and surface area of chemically activated carbons. *Microporous Mesoporous Mater.* **2008**, *115*, 603−608.
(12) Ben, T.; Ren, H.; Ma, S.; Cao, D.; Lan, J.; Jing, X.; Wang, W.; Xu, J.; Deng, F.; Simmons, J. M.; Qiu, S; Zhu, G. Targeted Synthesis of a Porous Aromatic Framework with High Stability and Exceptionally High Surface Area. *Angew. Chem., Int. Ed. Engl.* **2009**, *48* (50), 9457−60.
(13) Lan, J.; Cao, D.; Wang, W.; Ben, T.; Zhu., G. High-Capacity Hydrogen Storage in Porous Aromatic Frameworks with Diamond-like Structure. *J. Phys. Chem. Lett.* **2010**, *1*, 978−981.
(14) Yuan, D.; Lu, W.; Zhao, D.; Zhou, H-C. Highly Stable Porous Polymer Networks with Exceptionally High Gas-Uptake Capacities. *Adv. Mater.* **2011**, *23*, 3723−3725.
(15) Lu, W.; Yuan, D.; Zhao, D.; Schilling, C. I.; Plietzsch, O.; Muller, T.; Brase, S.; Guenther, J.; Blumel, J.; Krishna, R.; Li, Z.; Zhou, H-C. Porous Polymer Networks: Synthesis, Porosity, and Applications in Gas Storage/Separation. *Chem. Mater.* **2010**, *22*, 5964−5972.
(16) Xu, Y.; Chen, L.; Guo, Z.; Nagai, A.; Jiang, D. Light-Emitting Conjugated Polymers with Microporous Network Architecture: Interweaving Scaffold Promotes Electronic Conjugation, Facilitates Exciton Migration, and Improves Luminescence. *J. Am. Chem. Soc.* **2011**, *133*, 17622−17625.
(17) Garibay, S. J.; Weston, M. H.; Mondloch, J. E.; Colón, Y. J.; Farha, O. K.; Hupp, J. T.; Nguyen., S. T. Accessing functionalized porous aromatic frameworks (PAFs) through a de novo approach. *CrystEngComm* **2013**, *15*, 1515−1519.
(18) Lu, W.; Yuan, D.; Sculley, J.; Zhao, D.; Krishna, R.; Zhou, H-C. Sulfonate-Grafted Porous Polymer Networks for Preferential CO_2 Adsorption at Low Pressure. *J. Am. Chem. Soc.* **2011**, *133*, 18126−18129.
(19) Cossi, M.; Gatti, G.; Canti, L.; Tei, L.; Errahali, M.; Marchese, L. Theoretical Prediction of High Pressure Methane Adsorption in Porous Aromatic Frameworks (PAFs). *Langmuir* **2012**, *28*, 14405−14414.
(20) Yamazaki, T.; Watanuki, I.; Ozawa, S; Ogino, Y Infrared Spectra of Methane Adsorbed by Ion-Exchanged ZSM-5 Zeolites. *Langmuir* **1988**, *4*, 433−43.
(21) Chen, L.; Lin, L.; Xu, Z.; Zhang, T.; Liang, D. Interaction of methane with surfaces of silica, aluminas and HZSM-5 zeolite. A comparative FT-IR study. *Catal. Lett.* **1995**, *35*, 245−258.
(22) Kishima, M.; Okubo, T. Characterization of Microporous Titanosilicate ETS-10 by Infrared Spectroscopy with Methane as a Probe Molecule for Basic Sites. *J. Phys. Chem. B* **2003**, *107*, 8462−8468.
(23) Li, C.; Li, G.; Xin, Q. FT-IR Spectroscopic Studies of Methane Adsorption on Magnesium Oxide. *J. Phys. Chem.* **1994**, *98*, 1933−1938.
(24) Yoshida, H.; Yamazaki, T.; Ozawa, S. IR Spectra of CH_4 Physisorbed on an Active Carbon at Low Temperature. *J. Colloid Interface Sci.* **2000**, *224*, 261−264.
(25) Lubezky, A.; Chechelnitsky, L.; Folman, M. IR spectra of CH_4, CD_4, C_2H_4, C_2H_2, CH_3OH and CH_3OD adsorbed on C_{60} films. *J. Chem. Soc., Faraday Trans.* **1996**, *92* (12), 2269−2274.
(26) Wilson, L. M.; Griffin, A. C. Synthesis of molecular 'jacks': rigid tetrahedral molecules with p-phenylene arms. *J. Mater. Chem.* **1993**, *3*, 991−994.
(27) Fraccarollo, A.; Canti, L.; Marchese, L.; Cossi, M. Monte Carlo Modeling of Carbon Dioxide Adsorption in Porous Aromatic Frameworks. *Langmuir* **2014**, *30*, 4147−4156.
(28) Socrates, G. *Infrared and Raman Characteristic Group Frequencies: Tables and Charts*, 3rd ed.; John Wiley & Sons Inc: New York, 2004; pp 157−161.
(29) Colthup, N. B.; Daly, L. H.; Wiberley, S. E. Introduction to Infrared and Raman Spectroscopy. *Introduction to Infrared and Raman Spectroscopy*; Academic Press: New York, 1964; pp 261−280.
(30) Morita, S.; Fujii, A.; Mikami, N.; Tsuzuki, S. Origin of the Attraction in Aliphatic C-H/π Interactions: Infrared Spectroscopic and Theoretical Characterization of Gas-Phase Clusters of Aromatics with Methane. *J. Phys. Chem. A* **2006**, *110*, 10583−10590.
(31) Shimanouchi, T. *Tables of Molecular Vibrational Frequencies, Consolidated Volume I*; National Standard Reference Data Series; National Bureau Of Standards: Washington DC, 1972; Vol. *39*, pp 45−47.